

Stable Operation of PV Plants to Achieve Fault Ride Through Capability

Evaluation in Field and Laboratory Tests

Gregor Dötter, Florian Ackermann, Nicolas Bihler, Robin Grab, Soenke Rogalla, Roland Singer

Fraunhofer Institute for Solar Energy Systems ISE
Heidenhofstraße 2, 79110 Freiburg, Germany
gregor.doetter@ise.fraunhofer.de

Abstract— This paper first explains the required feed-in of voltage supporting currents during grid faults in a simplified case. Secondly, resonance points of the grid connection point are calculated analytically. The influence of weak grid conditions and large numbers of inverters is analysed. To underline the theoretical discussion on test conditions, measurements concerning Low Voltage Ride Through (LVRT) and stable operation of PV plants are presented. They comprise measurements from single inverters, as well as from large PV plants in the megawatt range.

Keywords—*Fault Ride Through, grid impedance, resonance point, LCL filter, field and laboratory test, PV plant, grid stability, voltage support, measurement results*

I. INTRODUCTION

In many electrical grids worldwide, the rising amount of installed PV power entails a considerable influence of PV systems on grid quality and stability. All indicators point to an increasing trend towards power electronic generation units. Both wind and solar plants have reached power levels comparable to conventional power plants. Considerable shares of renewable generation occur quite regularly throughout the world, not only in the German grid (e.g. ~50% at 21.July 2013, [16]). The ongoing substitution of synchronous generators by power electronic driven generation units require that those generation units guarantee the same level of stability and grid control functions. At Fraunhofer ISE's Megawatt Inverter Laboratory, several dozens of large PV inverters, with a nominal power of up to 1 MVA, have been characterised during the past four years. These measurements were expanded to fault ride through field tests in a 5 MW solar test plant. Solar power stations can be built up out of hundreds to even thousands of inverters running in parallel; therefore high requirements apply to the inverter's control algorithms. This paper discusses the various characteristics of grid connection points in large scale PV power plants and their impact on the system stability. Critical issues of the Fault Ride Through Test also examines the inverters performance in weak grid conditions. We present measurement results of both Low Voltage Ride Through (LVRT) field and laboratory measurements. To summarise, the performance of today's inverters will be compared with the needs of the future energy generation system and with the requirements of currently applicable international grid codes.

II. NECESSITY OF DYNAMIC GRID SUPPORT

A. Fault handling in today's electrical energy system

The transition of the electrical energy system towards a grid dominated by inverters requires a shift of responsibility and grid control capability towards PV inverters and wind turbines. The basis of the present protective system is a high short circuit power at the transmission level combined with a cascaded and staggered arrangement of protection devices at significant knots. This allows the grid protection device, which is the closest to the fault, to react and clear the fault. Due to the size of conventional power plants, the feed-in is at the highest voltage level and the energy is transferred to the consumers via the lower voltage levels.

B. Fault handling in power electronic dominated electrical energy systems

The inverters capability of supplying reactive current allows supporting of the grid voltage during the fault. First this reduces the impact of the fault onto nearby power consumers and secondly the inverters participate in the provision of short circuit current. Grids with a high share of power electronic loads and generation units will have a highly decentralised structure. Renewable energy sources usually form blocks in a smaller power range and require higher numbers of energy sources. They often feed into low and medium voltage levels. Any power electronic based generator has no or very limited over load capability unlike rotating machines or transformers. Power electronic generators also do not have an intrinsic inertia. Today's grid protection system is based on high fault currents; fault currents slightly higher than the nominal current are difficult to detect by the protection devices. To ensure a quick clearing of faults by grid protection devices each generation unit, including the distributed ones, need to provide dynamic grid support by feeding fault current into the grid.

The following calculation shall show how effective the feed-in of capacitive fault current is. A simple grid is presented in Fig. 1. The ideal grid is represented by a voltage source. The fault, represented by a variable load, is located at the end of a long inductive transmission line. This end is also fed by a PV inverter [12].

In a first case, the PV inverter is disabled. The resulting voltage V_{FAULT} at the end of the transmission line is now defined by the line impedance and the fault impedance.

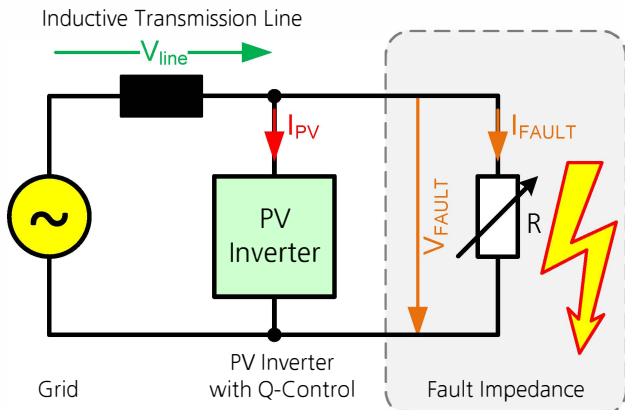


Fig. 1. Grid model to demonstrate the capability of the PV inverter to support the voltage V_{FAULT} .

The variation of the fault impedance is shown in the dotted yellow line in Fig. 2. The power transferred over the transmission line (or the power dissipation in the fault) reaches a maximum when the impedances have the same absolute value. At that operating point $V_{FAULT} = 1 p.u. / \sqrt{2} \approx 71\%$.

When the inverter is enabled the current I_{PV} influences the voltage V_{FAULT} at its terminals. If the inverter feeds active current into the grid fault, the influence on the grid voltage is almost negligible (red line compared to yellow line in Fig. 2). In the considered model, the transmission line is dimensioned to reach a short circuit power of 40 times the inverter power at its end. This can also be expressed in a short circuit ratio of $S_{short\ circuit} / P_{inverter} = 40$. The blue and the green line in Fig. 2, show the influence of the phase angle of I_{PV} onto the voltage V_{FAULT} and the power dissipation of the fault. Bearing in mind that a high fault current is needed to clear the fault as fast as possible, it is made visible in the green line that only capacitive fault current helps to support the grid voltage in inductive grids.

If a power electronic dominated grid consists of a large number of generation units, one can assume that many of them operate in part-load mode and can deliver higher fault currents (nominal current) than their present/actual current at the particular moment. This can be compared to a limited over-load capability. In micro grids with only few generation units, the voltage stability (voltage support corresponds to capacitive current) needs to be balanced against the frequency stability and the need for active current.

III. INTERNATIONAL GRID CODES

Grid codes ([8], [9], [10]) usually contain chapters on static grid support, dynamic grid support and grid protection. Static grid support mainly deals with the control of active and reactive power according to set points by the grid operator or control functions (e.g. $Q = f(V)$ or $\cos(\varphi) = f(P)$).

A. International Fault Ride Through Requirements

In dynamic grid support, many international grid codes distinguish between synchronous generators (type 1) and other generators (type 2), for example, PV and wind inverters. For type 2 generators most grid codes define the behaviour during the fault with set points for active or reactive current.

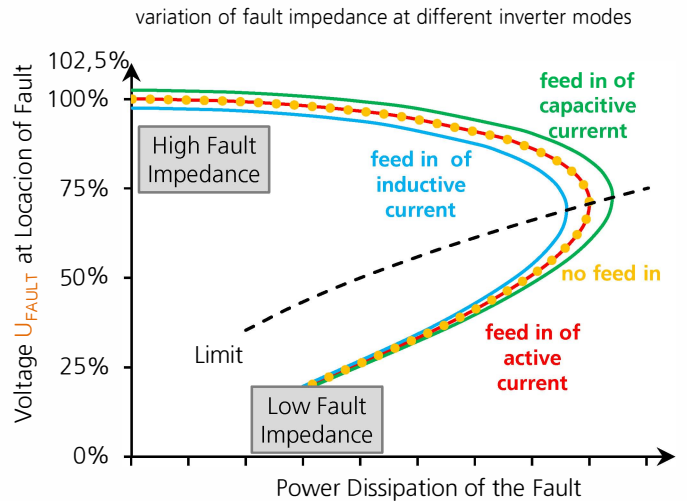


Fig. 2. Power dissipation of a grid fault at different fault impedances printed versus V_{FAULT} . The different color coded lines indicate the operation modes of the PV inverter. At capacitive feed-in (green line), the voltage is supported in the most effective way and the influence on neighbouring customers/loads is minimised.

After the fault response times define how fast the unit must return to the operation point before the fault. Quite often those requirements are not very detailed and rather tend to reduce the impact of power electronic sources than use their capabilities. For instance, requirements are given for three phase (= symmetric) faults and not for the more frequent asymmetric faults.

Generally speaking, fault ride through requirements are a contrary to the grid protection. The first one intends to keep the generation unit connected to the grid, whereas grid protection means the opposite, disconnection from the grid. Those two opposing functions are usually decoupled by time constants.

Future requirements for power electronic dominated grids, such as limitation of power gradients, phase shifter mode / Q at demand, primary control, balancing of the three phases (negative sequence control), damping of sub-harmonic oscillations and harmonics, black start capability, island operation mode of subnets, resynchronisation after islanding and communication interfaces / protocols still need to be defined and developed.

IV. IMPEDANCE DETERMINATION OF GRID CONNECTION POINT

The grid impedance is defined by any electrical equipment connected to the grid (e.g. generators, loads, transformers, cables...). All together they form a complex impedance which typically contains resonance points. In most cases, only the grid impedance at 50 Hz is known. This chapter will present an analytic approach to identify basic dependencies of the resonance points from the grid connection point and inverter specifications. At the planning stage of a PV or wind plant, the grid impedance is mostly exclusively used to calculate the maximum connectable power. The influence of the grid impedance onto the damping of harmonics, the interaction with the inverters grid filter and the resulting resonance points are often considered as subordinate.

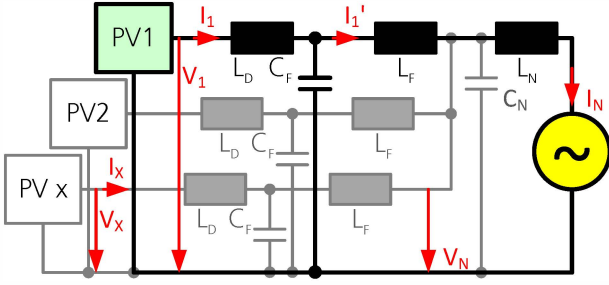


Fig. 3. Relevant components of the equivalent circuit at the grid side of a PV plant in a single line diagram.

A. Calculation of LCL Grid Filter Resonance

To discuss the resonances of the grid connection point in a PV plant the circuit in Fig. 3 is used [13]. The power electronic parts of the inverters are symbolised by $PV_1 \dots PV_x$ in Fig. 3. The rectangular shaped output voltages $V_1 \dots V_x$ of the IGBT stage is filtered by the inverters internal LC filter ($L_D; C_F$). It is common practice in the field of central inverters to use only an internal LC filter and to extend the filter with the stray / leakage inductance of the feed-in transformer L_F to a LCL filter.

In a first step the grid impedance is only characterised with the impedance L_N . The capacitive influence of cables and overhead lines is later modeled by the capacity C_N . To simplify the calculation any resistive components are neglected.

By neglecting of the grey components in Fig. 3 the output voltage of the IGBT stage V_1 is transferred to the grid current I_N with the following function:

$$H_1(j\omega) = \frac{I_N}{V_1} \frac{-1}{j\omega(L_D + L_F + L_N) - j\omega^3(C_F L_D(L_F + L_N))} \quad (1)$$

The resonance point of $H_1(j\omega)$ is:

$$\omega_1 = \sqrt{\frac{L_D + L_G}{C_F L_D L_G}} \text{ with } L_G = L_F + L_N \quad (2)$$

A parallel connection of x inverters (printed in grey in Fig. 3) leads to a transfer function similar to $H_1(j\omega)$. Note that the cable capacity C_N is still neglected.

$$H_x(j\omega) = \frac{I_N}{\sum_{i=1}^x V_i} \frac{1}{j\omega(L_D + L_F + xL_N) - j\omega^3(C_F L_D(L_F + xL_N))} \quad (3)$$

Again, the resonance point of $H_x(j\omega)$ shows a similar structure:

$$\omega_x = \sqrt{\frac{L_D + L_G}{C_F L_D L_G}} \text{ with } L_G = L_F + x \cdot L_N \quad (4)$$

The dependency of the resonance point ω_x from the grid impedance L_N and the number x of inverters in parallel has an influence on the grid side behaviour of inverters $PV_1 \dots PV_x$.

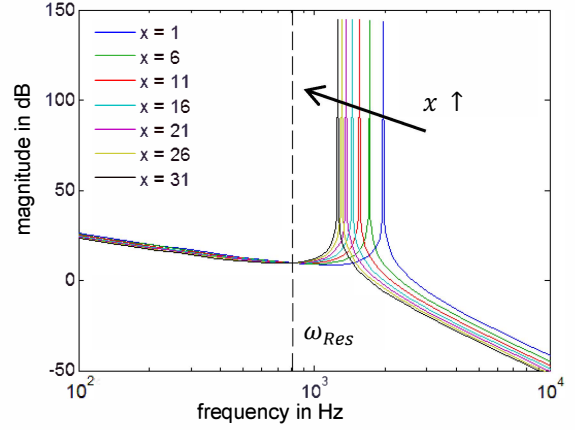


Fig. 4. Magnitude plot of $H_x(j\omega)$ at different numbers x of inverters. The resonance point is shifted to lower frequencies at a high number of inverters.

At weak grid conditions the value L_N rises and thus the value of L_G . An increase of the number x of inverters also increases L_G . Both effects lead to a shift of the resonance point ω_x towards lower frequencies [1]. ω_x converges towards ω_{RES} :

with $x \uparrow$ and $L_N \uparrow$

$$L_G \gg L_D \Rightarrow \omega_{RES} = \frac{1}{\sqrt{C_F L_D}} \quad (5)$$

The boundary value ω_{RES} is the minimum value of ω_x at very weak grid conditions and a very high number of inverters. It is only defined by the two inverter internal LC filter components L_D and C_F and always known by the inverter manufacturer.

B. Impact of the Number of Inverters on the LCL Filter Resonance

Fig. 4 shows the shift of the LCL filter resonance when several inverters are operated in parallel in a PV plant. The grid impedance L_N was chosen for strong grid conditions with a short circuit ratio of $S_{short\ circuit}/(15 * P_{inverter}) = 50$. The dashed line indicates the minimum value of the resonance point ω_{RES} . For the calculation of the magnitude plots the following values were assumed: $L_D = 5 \mu H$; $C_F = 600 \mu F$; $L_F = 12 \mu H$.

C. Impact of the Grid Impedance on the LCL Filter Resonance

Similar to Fig. 4 and also in Fig. 5 a convergence of the resonance point towards ω_{RES} can be recognised. In Fig. 5, the grid impedance L_N was varied from a short circuit ratio $S_{SC}/P_{plant} = 50$ (strong grid conditions, blue line in Fig. 5) to $S_{SC}/P_{plant} = 5$ (weak grid conditions, black line in Fig. 5). Both effects, weak grid conditions and a large number of inverters are usually present at the same time in large PV plants, whereas in small plants the number of inverters is low and the grid conditions are usually stronger. This results in a large interval for the resonance point ω_x at possible grid connection points and sets high demands onto the control of the inverters.

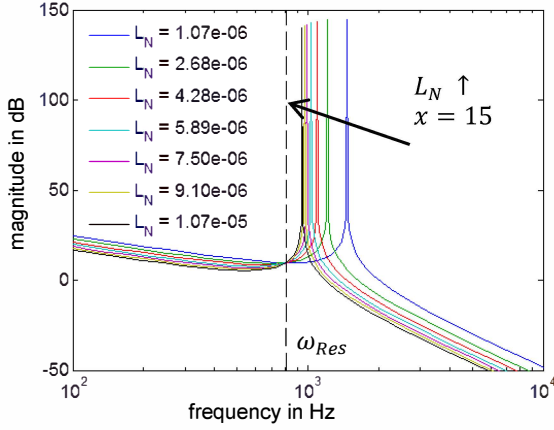


Fig. 5. Magnitude plot of $H_x(j\omega)$ at different values of the grid impedances L_N and $x = 15$ inverters. The resonance point is shifted to lower frequencies at weak grid conditions.

Laboratory, as well as field measurements, showed that the control algorithms of the inverters are not always stable within this wide range of the resonance point. The consequences of non-sufficient stability [2] vary between higher values of harmonics or flicker up to disconnections of several inverters [3]. In line with that, a loss of feed-in, inverter failures or unwanted disconnections during grid faults take place. To ensure a stable operation of PV plants the number of parallel units and the range of the grid impedance must be taken into account while dimensioning the grid filter and designing the inverters current controller [4], [7]. In addition, methods of active damping can be used [5].

D. Impact of the Medium Voltage Cabeling on the LCL Filter Resonance

The cable capacitance C_N shown in Fig. 3 adds a second resonance point to the transfer function [6]. Because of the short distances between the inverter stations in a plant, the series influence of the cable can be neglected and the equivalent circuit can be simplified to capacitor connected in parallel. To calculate the value of C_N , the total length of the medium voltage cable is relevant. The two resulting resonance points can be estimated with the following two equations:

$$\omega_{HF} \approx \sqrt{\frac{1}{C_N} \frac{L_F + xL_N}{L_F L_N} + \frac{L_D + L_F}{C_F L_D L_F}} \quad (6)$$

$$\omega_{LF} \approx \sqrt{\frac{L_D + L_F + xL_N}{C_N L_N (L_D + L_F) + C_F L_D (L_F + xL_N)}} \quad (7)$$

Both estimations and Fig. 6 show that for large cable capacitances C_N , the resonance points are again shifted to lower frequencies. The resonance point ω_{HF} can be in the range of the switching frequency of central inverters.

The damping of the transfer functions at their resonance points is difficult to calculate because resistive components are often unknown. It was further reported, that the currents needed for charging the medium voltage cable capacitance of a disconnected wind plant exceeded the limits for harmonics.

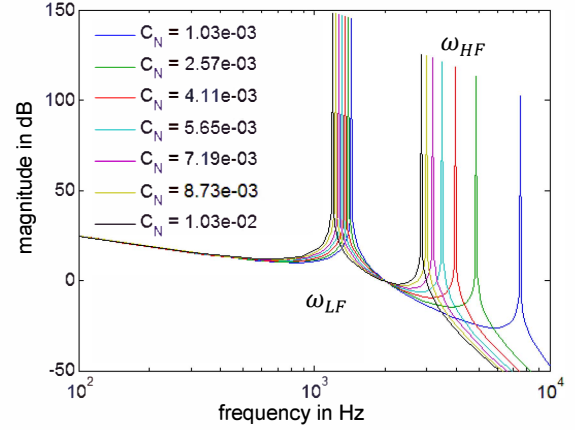


Fig. 6. Magnitude plot of $H_{x,N}(j\omega)$ at different lengths of medium voltage cables (1 km until 10 km) and $x = 15$ inverters. The resonance point is shifted to lower frequencies at high cable length.

In Fig. 3 the transformers were modelled with their stray impedance L_F . The equivalent T-circuit was not used because the magnetic impedance of the transformer can be neglected in this case. Moreover the grid impedance angle ψ was also not considered.

V. LOW VOLTAGE RIDE THROUGH (LVRT) MEASUREMENT RESULTS

Any test setup shall be as close as possible to reality. Unfortunately, most of the requirements of the grid codes are not / cannot be tested in real operation conditions. It is common practice to test a single generation unit and later extrapolate the measurement results onto the behaviour of an entire plant. This chapter will first discuss test conditions, setups and later focus on measurement results achieved in field and laboratory.

A. Comparison of Laboratory and Field Measurement Test Conditions

According to the German and other grid codes, it is allowed to test PV inverters in a laboratory. The PV modules can be simulated by a DC source. Test laboratories are often characterised by a strong grid connection point with a high short circuit power. Quiet often there are loads connected to the same grid connection point. Those loads provide a certain damping for harmonics. Due to reasons of complexity, most of the time only a single inverter is tested. A typical laboratory test setup is shown in Fig. 7.

Fig. 8 describes a typical setup of large PV plants. Large plants are often built in rural areas at weak grid connection points. If they are directly connected to the high voltage grid, the high relative short circuit voltage v_k of the high voltage transformer also results in weak grid conditions. The range of v_k for high voltage transformers (i.g. 110 kV/20 kV; 40 MVA) usually varies from 12 to 18, which results in a short circuit ratio between 5.6 and 8.3 and represents weak grid conditions [14]. Often there are no loads directly connected at the high voltage grid connection point of large plants, and this can result in a lag of damping. The entire length of the internal medium voltage cable network of the plant adds up as a capacity (represented by C_N in Fig. 3).

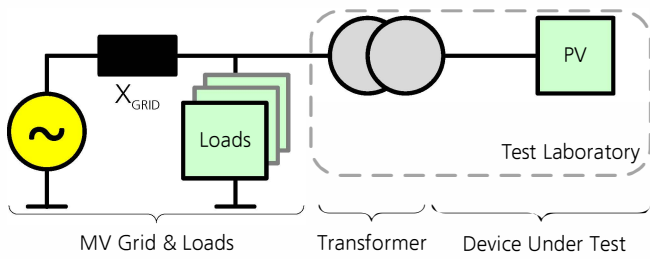


Fig. 7. Typical laboratory test setup for a single inverter including several loads at a strong grid connection point.

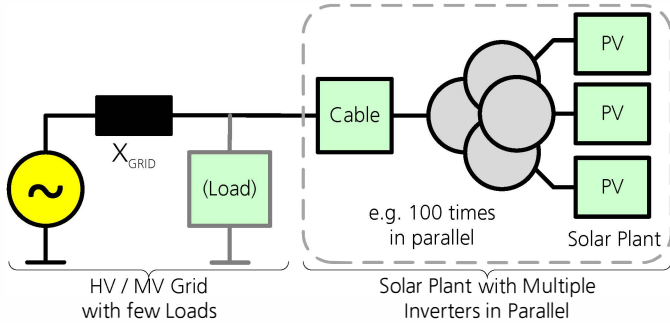


Fig. 8. Typical setup of a large PV plant which is characterised by a weak grid connection point, the absence of/few loads, MV cable networks, transformers with multiple low voltage windings and a large number of inverters.

The transformers used for PV inverters often contain two or three low voltage windings. Which are used for the galvanic isolated connection of several inverters to a single transformer. Large PV plants consist of several hundreds of inverters running in parallel. The large number is a very unique phenomenon for PV. For wind and other renewable sources fewer units are clustered. Not all of these singularities can be included in laboratory test setups but they are implemented as well as possible.

B. LVRT Testbench: Inductive Voltage Divider

To prove the LVRT capability a test bench is needed. Fig. 9 shows an LVRT test bench based on an inductive voltage divider [11]. The ratio of X_{Line} and X_{SC} defines the level of the voltage drop. The circuit breakers activate or bypass their corresponding impedances. This test bench is located on the medium level and widely used for testing the LVRT capability of PV and wind generation units. Alternative test facilities shall not be discussed in this paper.

C. GPS Synchronised Measurement System

Any LVRT result presented later on was carried out with a test bench according to Fig. 9. The measurements were done with a GPS synchronised data acquisition system. Fig. 10 shows the five measurement units which are each synchronised by an individual GPS receiver. Each unit can sample up to 16 channels at a sampling rate of 50 kHz. The data is either transferred via a Wi-Fi transmission or by Ethernet to a central data server, where the all the data is stored and analysed.

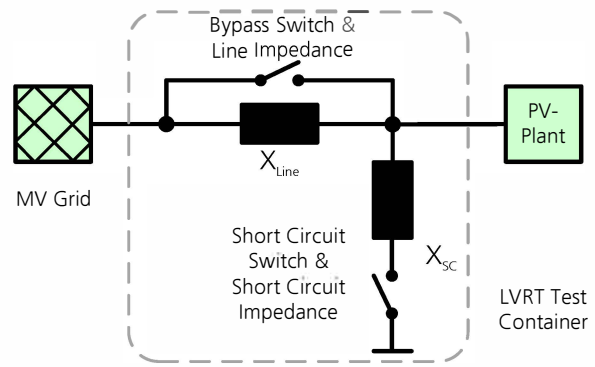


Fig. 9. Single line diagram of an inductive voltage divider used as an LVRT test bench.

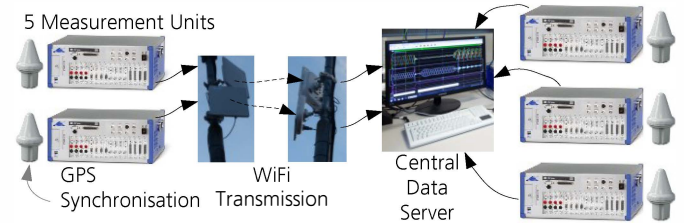


Fig. 10. GPS synchronised data acquisition system.

D. LVRT Laboratory Measurement – Comparison of Multiple Inverters

As discussed earlier on in the chapter on grid codes the guidelines give very strict regulation in some cases, but also weak regulations in other points. Fig. 11 shows measurement results of 16 different central inverters during a voltage drop to 0.25 per unit. Precise definitions in the grid codes for the control of the reactive current of the positive sequence lead to a very uniform behaviour (bottom diagram of Fig. 11).

The German grid code set no definitions for the control of the active current of the positive sequence. As a consequence, the measurement results in the top diagram of Fig. 11 are non-uniform. It is problematic that some inverters need 1.5 s or longer to get back to nominal current after the fault. Nevertheless, this is still compliant with the German grid code. Other grid codes set stricter regulations in this area.

E. LVRT Laboratory Measurement of 4 Parallel Inverters

Due to their LVRT behaviour, four central inverters were assessed at Fraunhofer ISE's Megawatt Laboratory. Each 100 kW central inverter contained an internal transformer so that the devices under test could be directly connected at the low voltage terminals. Fig. 12 presents a voltage drop to 0.5 per unit. The top section of the diagram shows the voltage at the connection point at low voltage level. The individual current of each inverter is printed in the four bottom sections of Fig. 12. The sum of the four currents is shown in the second section (total current). At the beginning of the fault 2 pulse blocking phases (no switching of IGBT's) can be seen. They are indicated by the two green arrows. While testing of only one inverter the fault current could be raised faster and with just one short pulse blocking phase. In Fig. 12 the settling times for the required capacitive fault current could not be met due to the second pulse-blocking phase.

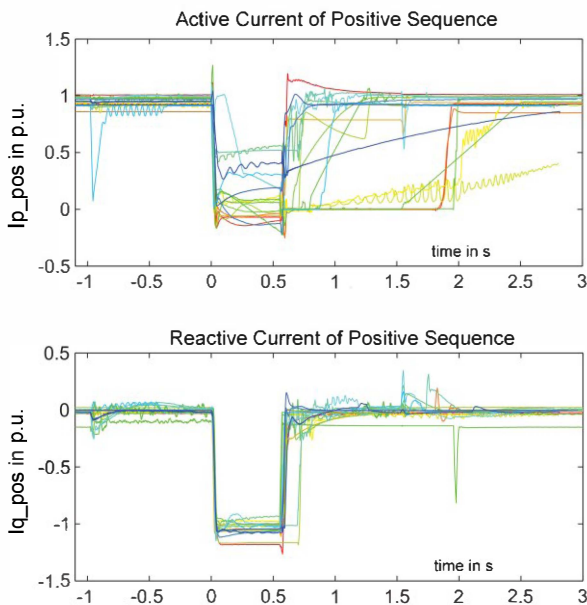


Fig. 11. Comparison of the current feed-in of 16 central inverters during a voltage drop to 0.25 per unit ($t = 0 - 0.5$ s). Top diagram: weak requirements for the control of the active current result in a non uniform behavior of the 16 shown inverters. Bottom diagram: precise requirements for the control of the reactive current result in an uniform behavior. Each colour represents one type of central inverter.

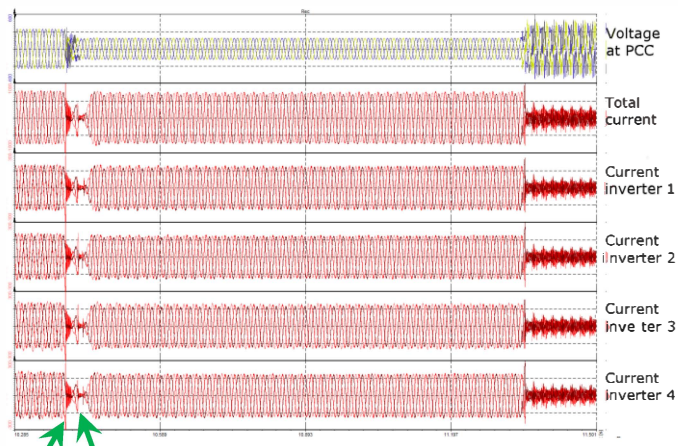


Fig. 12. Voltage drop to 0.5 p.u. of four central inverters. The inverters were directly connected at low voltage level and contained an internal low voltage transformer. The green arrows each indicate a pulse blocking phase of the two inverters. Scaling: voltage at PCC = ± 600 V; total current = ± 1000 A; inverter current = ± 300 A; time ≈ 1.25 s.

Other types of inverters manage to ride through a fault with a continuous current. After the fault, the grid voltage is distorted due to the inrush of the feed-in transformer. The tested inverters raised their current after the attenuation of the inrush effect.

F. LVRT Field Measurement of a 5 MW Solar Plant

To assess the fault ride through capability of PV inverters not just in the test laboratory, an LVRT field test was carried out in a 5 MW test plant. This test plant consists of five one megawatt substations.

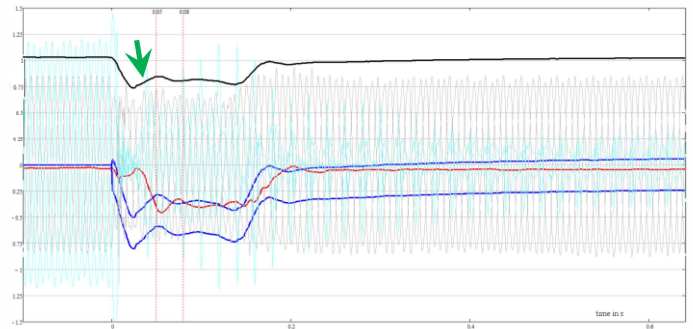


Fig. 13. Voltage drop to 0.73 p.u. measured at the low voltage terminals of one inverter in a substation. Black: positive sequence of the grid voltage; Red: reactive current of the positive sequence; Blue: tolerance band around the set point for the reactive current. Turquoise: instantaneous values of the grid current; Grey: instantaneous values of the grid voltage. Scaling: per unit values; time ≈ 0.7 s.

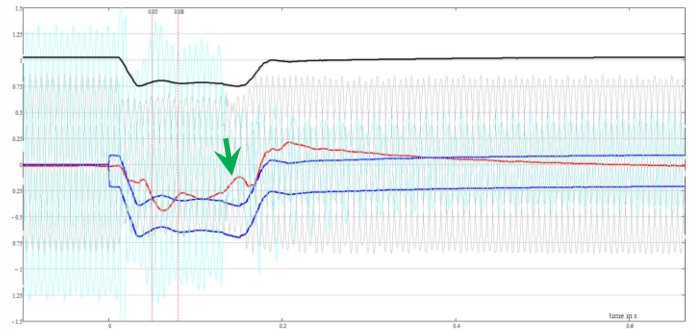


Fig. 14. Voltage drop to 0.73 p.u. measured at the LVRT test container at medium voltage level. Black: positive sequence of the grid voltage; Red: reactive current of the positive sequence; Blue: tolerance band around the set point for the reactive current. Turquoise: instantaneous values of the grid current; Grey: instantaneous values of the grid voltage. Scaling: per unit values; time ≈ 0.7 s.

Each substation contained one medium voltage transformer with three windings on the low voltage side connected to three 350 kW central inverters. The measurement system presented in Fig. 10 was installed in four of the substations and in the LVRT test container. Fig. 13 presents measurement results acquired at the low voltage terminals of one inverter in a substation and Fig. 14 shows the measurement data acquired at the same time in the LVRT test container at the medium voltage connection point of the 5 MW plant. The red line in Fig. 13 shows the reactive current of the positive sequence. It reaches its set point (blue tolerance band) within the required time span of 50 ms, but settles around the minimum tolerance band and even goes below the tolerance band within the fault. The grid supporting effect of the capacitive fault current onto the positive sequence of the grid voltage (black line in Fig. 13) is indicated by the green arrow.

Fig. 14 shows a similar behaviour of the entire 5 MW plant. However towards the end of the grid fault some units stopped delivering the required capacitive current. This is why the capacitive fault current of the positive sequence (red line in Fig. 14) missed the tolerance band (green arrow in Fig. 14).

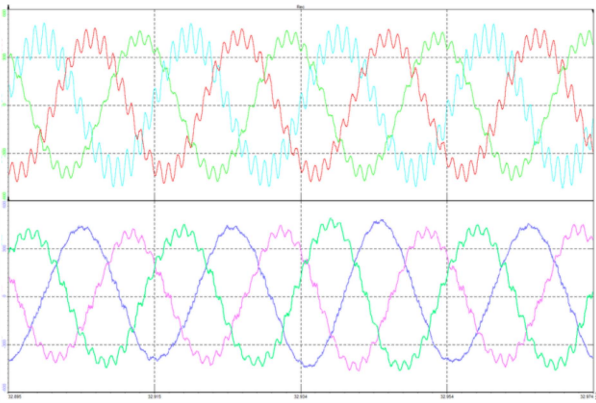


Fig. 15. Oscillation at the resonance frequency of the grid filter. Top Diagram: instantaneous values of the grid voltage at inverter terminals. Bottom Diagram: instantaneous values of the grid current at inverter terminals. Scaling: voltage = ± 600 V; current = ± 600 A; time ≈ 0.08 s.

These measurements show that the majority of the inverters can successfully ride through a grid fault, deliver the required capacitive fault current and raise the active power after the fault to the level before the fault, but it is still an obvious demonstration that the measurement of a single generation unit is not evidence of a successful LVRT at plant level. The extrapolation of measurement results from the certification of power generation units to the plant level needs to be treated with caution.

VI. MEASUREMENT RESULTS CONCERNING STABLE OPERATION OF PV PLANTS

This chapter will show results where the stable operation of large plants was not given [15].

A. Oscillations at LCL Grid Filter Resonance Frequency

The measurement shown in Fig. 15 contains a high harmonic component (~ 850 Hz) at the resonance frequency of the grid connection point. These oscillations were triggered under artificial, but not untypical, weak grid conditions. The line inductor of a LVRT test container (X_{Line} in Fig. 9) was used to simulate weak grid conditions. During the measurement a sound caused by the oscillation was could be heard in the entire plant. Although this measurement was generated under artificial conditions, this phenomenon has been reported to a limited extent by many inverter manufacturers.

B. Sub-harmonic Oscillations at Grid Connection Point

Oscillations can take place at different frequencies. The field of harmonics and other oscillations at frequencies greater than the fundamental frequency is mostly better known as the sub-harmonic range below the grid frequency. It is easier to measure and detect harmonics in a test bench. They can also be provoked by certain methods (extra line inductor or extra parallel capacitor) and investigated then. Sub-harmonic effects were reported at large numbers of inverters, which are difficult to include in a test setup.

As presented earlier on in Fig. 3 the grid connection point consists of several components with energy storage. Capacitors store energy in their electric field and inductors in their magnetic field respectively. If two types of energy storages are combined, an oscillation system is formed.

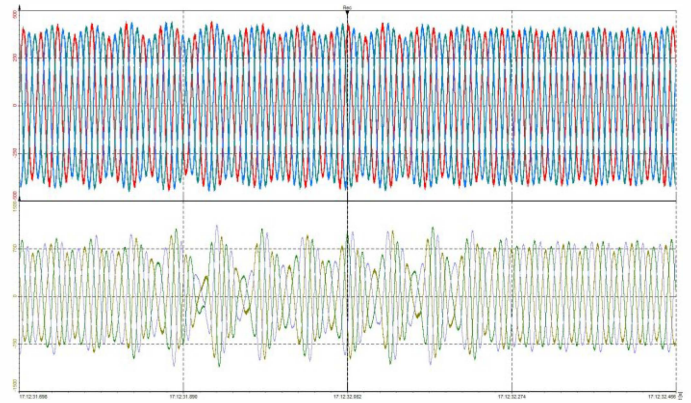


Fig. 16. ~ 25 Hz oscillation in a large PV plant. Top diagram: AC voltage; Bottom diagram: AC current, both measured at the inverter terminals of a central inverter. Scaling: voltage = ± 500 V; current = ± 1500 A; time ≈ 0.78 s.

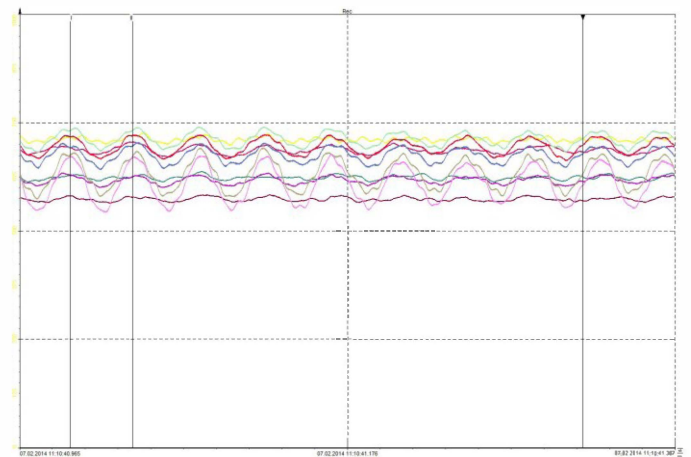


Fig. 17. DC voltages during a ~ 25 Hz oscillation in a large PV plant. The synchronous oscillation of each inverter can be seen in this figure. Normally, the DC voltage should be flat. Scaling: 0 - 1000 V; time ≈ 0.42 s.

The integral components of the control algorithms of the inverters also form a kind of “virtual storage”. Altogether, in large plants, the three types of storage elements form a common oscillation system. It is very difficult and still under research, to identify typical time constants, basic principles, propagation mechanisms and counter methods to fight oscillations in parks.

Fig. 16 presents a measurement in a PV plant greater than 40 MW. The setup of the plant is typical and also common in other plants at a similar power level. The top diagram of Fig. 16 shows the oscillation of the voltage at the AC terminal of an inverter at low voltage level. This inverter was located very close to the grid connection point. The sub-harmonic oscillation at ~ 25 Hz could be measured at multiple inverters in the plant. No triggering event could be identified so far. The bottom diagram of Fig. 16 shows the corresponding current at the AC terminals of the inverter.

The oscillation presented above was also measurable at the DC side of the inverters. Fig. 17 shows a measurement of the DC voltage. It can be seen that the oscillation of any measured inverter is in phase.

VII. CONCLUSION

The LVRT measurement results presented above show the ability, of not only single inverters but also large plants to perform dynamic grid support. This paper shows results from the test of single inverters, small inverter clusters and large plants in the multi megawatt range. The measurements and the discussion of international grid codes give impulses for further improvements of the behaviour during grid faults. The analytic calculation of the resonance frequency of the grid connection point and the identification of influence factors provide valuable information for inverter manufacturers and control loop designers. The two measurements presented in the chapter on stable operation underline the importance of robust and oscillation damping control algorithms.

Although differences between common test setups and large PV plants were outlined, challenges for the inverter control faced in large plants are also tested with the presented LVRT test bench. The series impedance particularly proves the behaviour of generation units at weak grid conditions and the shift of resonance points.

ACKNOWLEDGMENT

Parts of this work were financed by the German federal ministry for economic affairs and energy under the project number 0325452.

REFERENCES

- [1] J. L. Agorreta, M. Borrega, and J. López, "Modeling and control of N -paralleled grid-connected inverters with LCL filter coupled due to grid impedance in PV plants," *IEEE Trans. Power Electron.*, vol. 26, no. 3, pp. 770-784, Mar. 2011.
- [2] L. Zhou, and M. Zhang, "Modeling and stability of large-scale PV plants due to grid impedance," *Industrial Electronics Society, IECON 2013 - 39th Annual Conference of the IEEE*, pp.1025-1030, 10-13 Nov. 2013.
- [3] J. H. R. Enslin, and P. J. M. Heskes, "Harmonic interaction between a large number of distributed power inverters and the distribution network," *IEEE Trans. Power Electron.*, vol.19, no.6, pp.1586-1593, Nov. 2004.
- [4] M. Liserre, R. Teodorescu, and F. Blaabjerg, "Stability of photovoltaic and wind turbine grid-connected inverters for a large set of grid impedance values," *IEEE Trans. Power Electron.*, vol.21, no.1, pp.263-272, Jan. 2006.
- [5] J. He, Y. W. Li, D. Bosnjak, and B. Harris, "Investigation and active damping of multiple resonances in a parallel-inverter-based microgrid," *IEEE Trans. Power Electron.*, vol.28, no.1, pp.234-246, Jan. 2013.
- [6] X. Lu, M. Liserre, K. Sun, F. Blaabjerg, R. Teodorescu, and L. Huang, "Resonance propagation of parallel-operated DC-AC converters with LCL filters," *Applied Power Electronics Conference and Exposition (APEC), 2012 Twenty-Seventh Annual IEEE*, pp.877-884, 5-9 Feb. 2012.
- [7] Y. Bae, T. K. Vu, R. Y. Kim, "Implemental control strategy for grid stabilization of grid-connected PV system based on german grid code in symmetrical low-to-medium voltage network," *IEEE Trans. Energy Conversion*, vol.28, no.3, pp.619-631, Sept. 2013.
- [8] Technical Guidelines for Power Generating Units, Part 3 Determining the Electrical Properties - Power Quality. Revision 23, FGW e.V., May 2013.
- [9] Technical Guidelines for Power Generating Units, Part 4: Determining the Electrical Properties - Power Plant Behaviour. Revision 4, FGW e.V., May 2013.
- [10] Generating Plants Connected to the Medium-Voltage Network : Guideline for generating plants connection to and parallel operation with the medium-voltage network, BDEW Bundesverband der Energie- und Wasserwirtschaft e.V., Jun. 2008.
- [11] Measurement and assessment of power quality characteristics of grid connected wind turbines, DIN EN 61400-21:2008 (IEC 61400-21:2008), Jun. 2009.
- [12] A. J. Schwab, "Elektroenergiesysteme: Erzeugung, Transport, Übertragung und Verteilung elektrischer Energie" Springer Berlin Heidelberg, Germany, ed. 3, 2012.
- [13] G. Dötter, N. Bihler, F. Ackermann, R. Singer, S. Rogalla, and B. Burger, "Analyse des Verbundbetriebs von PV-Zentralwechselrichtern während Netzfehlern," *ETG-Kongress*, Berlin, Germany, Nov. 2013.
- [14] G. Dötter, F. Ackermann, N. Bihler, R. Singer, S. Rogalla, and T. Schaupp, "Ist die dynamische Netzstützung in PV-Parks gewährleistet? Erfahrungen aus der Low-Voltage-Ride-Through-Vermessung eines 5-MW-Solarparks," *29. Symposium Photovoltaische Solarenergie*, Bad Staffelstein, Germany, Mar. 2014.
- [15] "Auch Solarparks sind vor Netzstörungen nicht sicher!," Grossen Metrawatt, Nürnberg, Germany, Dec. 2012.
- [16] B.Burger, "Stromerzeugung aus Solar- und Windenergie im Jahr 2013", Data on renewable energy generation in Germany, Fraunhofer ISE, Freiburg, Germany.